

A study of Ag additive methods by comparing mechanical properties between Sn57.6Bi0.4Ag and 0.4 wt% nano-Ag-doped Sn58Bi BGA solder joints

Huayu Sun · Qingqian Li · Y. C. Chan

Received: 7 May 2014 / Accepted: 14 July 2014 / Published online: 27 July 2014
© Springer Science+Business Media New York 2014

Abstract Sn–Bi solder was proposed as one of the most promising substitutes for lead solder due to its lower melting temperature, good wettability, good yield strength and cost efficiency. With Ag elements added, the mechanical properties of Sn–Bi solder were improved obviously. There are two ways that are commonly used to add the reinforced particles into the solder. The first way (Way I) is to blend the reinforced particles with solder powders together, and then followed by pressure forming, sintering, cooling, crystallization and serious machining methods under inert atmosphere to make the solder paste. Another way (Way II) is to directly add the reinforced nano or micro particles into the solder paste by sufficient mechanical-stirring. In this research we would like to get fully understanding on the effects of these two ways of Ag addition on the mechanical properties of Sn–Bi–Ag solder joints during aging. Sn57.6Bi0.4Ag solder stands for the Way I and the doped Sn58Bi + 0.4Ag solder stands for the Way II. These two kinds of joints were compared via micromorphology observation, thermal failure analyses as well as balls shear strength measurement after different aging time (under 100 °C, from 0 to 800 h). The mechanical properties of Sn57.6Bi0.4Ag and the doped Sn58Bi + 0.4Ag solder joints during aging were shown to be associated with the changes of micromorphology, the dissolution of IMCs, as well as the flatness of the joints' interface. Before long-time aging, the doped Sn58Bi + 0.4Ag solder joints showed better mechanical performance than Sn57.6Bi0.4Ag solder joints. During aging, Sn56.7Bi0.4Ag solder joints had better performance in preventing the dissolution of Ni–Sn IMCs into the solder

side, having smoother interfaces, comparing with Sn58Bi + 0.4Ag solder joints. The degenerated phenomenon of Ag nanoparticle reinforcement seriously happened in the doped Sn58Bi + 0.4Ag solder joints. After longtime aging, Sn57.6Bi0.4Ag solder joints had better mechanical properties than the doped Sn58Bi + 0.4Ag solder joints.

1 Introduction

For the new published regulations of environmental protection, Sn37Pb solder has been gradually forbidden since 2002. At the same time, lead-free solder starts to attain more attention and develops very quickly in recent years. Up to now, lead-free solder has already become the first-chosen material in electronic manufacturing fields. There are many kinds of lead-free solders available in different manufacturing processes, such as Sn–Ag–Cu, Sn–Ag, Sn–Cu, Sn–Zn and Sn–Au solder. Commonly used in wave and reflow soldering processes, these lead-free solders have a much higher melting temperature, comparing with Sn37Pb solder whose melting point is around 183 °C [1–3]. Therefore, the utilization of lead-free technology inevitably raises the cost of manufacturing and damages the high-temperature-sensitive print circuit boards and components. To solve these problems and develop the low temperature bonding technology, researchers have been pushing forward the study on Sn–Bi solder significantly in the past several years. In Japan, Sn58Bi solder is widely used in the industry and proposed as one of the most promising substitutes for lead solder. Because Sn58Bi solder has lower melting temperature around 139 °C, good wettability, good yield strength and cost-efficiency [4].

Meanwhile, owing to the miniaturization of the electronic devices, widespread concerns have been paid on

H. Sun (✉) · Q. Li · Y. C. Chan
Department of Electronic Engineering, City University of Hong Kong, Tat Chee Avenue, Kowloon, Hong Kong
e-mail: huayusun22@gmail.com

requirements for better mechanical and electrical performances and reliability of the joint between solder ball and pad [5]. Although lead-free solders make great contributions to the protection of environment, they have strict limits on the mechanical properties contrasting with Sn37Pb solder that has higher reliability. Sn–Bi solder is not an exception. Plenty of researches have been done to improve the mechanical properties of lead-free solder joints by addition of reinforced particles. These particles in the solder can hinder the lattice dislocation by blocking grain boundaries and form intermetallic compounds (IMCs) that have better characteristics, to make the grain finer and improve the resistant to thermal, mechanical and electrical stresses [6–8]. Metals, such as Ag, Au, Al, Ni, Cu, Cd, Zn, Mo and some rare-earth materials [9, 10], and non-metallic materials, such as SiC, TiO₂, Al₃O₂, carbon tube, graphen and even diamond [11–15], are studied as the doped particles to improve the mechanical properties of lead-free solder joints. According to these studies, there are two methods that are commonly used to add the reinforced particles into the solder. The first way (Way I) is to blend the reinforced particles with solder powders together, and then followed by pressure forming, sintering, cooling, crystallization and serious machining methods under inert atmosphere to make the solder paste [16]. It is as same as the way that used in the industry to fabricate solder pastes. Another way (Way II) is to directly add the reinforced nano or micro particles into the solder paste by sufficient mechanical-stirring. Up to now, plenty efforts have been done to improve the mechanical properties of Sn–Bi solder by adding Ag elements in it [17]. However, to our best knowledge, no study has been reported to detect the effect of Ag additive methods on the mechanical properties of Sn–Bi–Ag solder joints.

In this study, Sn57.6Bi0.4Ag ternary solder (Way I) was commercially available, and doped Sn58Bi + 0.4Ag solder (Way II) was prepared by dispersing 0.4 wt% nano Ag particles additive mechanically in the Sn58Bi solder paste. To get fully understanding on the effects of Ag addition method on the mechanical properties of Sn–Bi–Ag solder joints during aging, Sn57.6Bi0.4Ag and the doped Sn58Bi + 0.4Ag BGA solder joints were compared, via micromorphology observation, thermal failure analyses as well as balls shear strength measurement after different aging time (under 100 °C, from 0 to 800 h). This research provides clear explanations for the changes and the different results of these solder joints.

2 Experimental procedures

The Sn58Bi (ALPHA) eutectic solder paste and Sn57.6Bi0.4Ag (ALPHA) near eutectic solder paste were both commercially available. The doped Sn58Bi + 0.4Ag

Table 1 Chemical composition of the solders studied

Solder	Composition (wt%)		
	Sn	Bi	Ag
Sn58Bi	42.00	58.00	–
Sn57.6Bi0.4Ag	42.00	57.60	0.40
doped Sn58Bi + 0.4Ag	41.84	57.76	0.40 (nano particles)

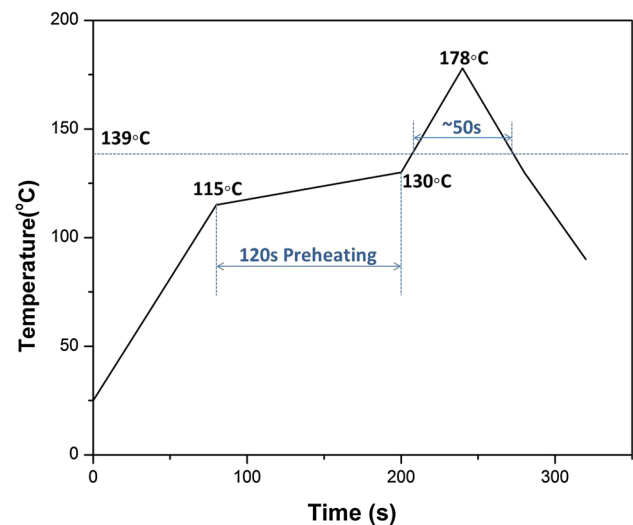


Fig. 1 The reflow program of Sn58Bi solder paste

solder paste was prepared by dispersing 0.4 wt% nano Ag particles (Xuzhou Jiechuang New Material Technology Co., Ltd.; purity of 99.9 %; average diameter of 70 nm; density 10.49 g/cm³) mechanically into Sn58Bi solder paste. To guarantee the Ag atoms weight percent in the pure Sn58Bi solder equals to 0.4 wt%, the weight of solder flux in the solder paste was subtracted out by calculation in the process of doping. The chemical compositions of the solders are summarized in Table 1. The blending process lasted more than 60 min to achieve a uniform distribution of nano Ag particles in the solder paste. And then these three kinds of solder pastes were printed onto alumina substrate using a 0.15 mm thick strain less stencil, and reflowed in the reflow oven (Pyramax-100N; BTU International) with peak temperature of 178 °C to make solder balls. The reflow program used in this research is shown in Fig. 1. After solidification, the solder balls were screened by the average diameter of 670 μm. The solder balls were attached onto the three-layer (Au/Ni/Cu) bump metal (UBM) pad of BGA chip, and then experienced a reflow process once more to make the joint specimens with the assist of solder flux to clean the oxidations on the pad. The cross-sectioned view of the specimens is shown in Fig. 2.

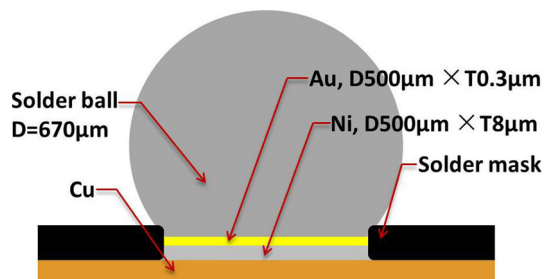


Fig. 2 The cross-sectioned view of the specimens. D diameter, T thickness

Differential scanning calorimeter (DSC, MDSC 2910) was used to determine the melting temperatures of Sn58Bi, Sn57.6Bi0.4Ag and doped Sn58Bi + 0.4Ag solders. The heating rate for the DSC test was set as 5 °C/min, and the range of test temperature was set from 100 to 180 °C.

To characterize the effect of the operating temperature on the micromorphology and the mechanical properties of the solder joints, specimens were isothermally aged under 100 °C, for 100, 200, 500, and 800 h respectively. After aging, the specimens were cross-sectioned and mounted in resin, then grounded with different grit sizes of emery papers and polished with diamond powder down to the size of 1.0 μm. Finally, the specimens were etched with 2.0 % dilute HCl for 10 s. Micromorphology analysis was taken by using a scanning electron microscope (SEM, Philips XL 40 FEG) in backscattered electron image mode to observe the cross-sectioned solder joints. And an energy dispersive X-ray spectrometer (EDX, International, DX-4) was utilized to determine the chemical compositions of IMCs. The accuracy of the compositional measurements was typically $\pm 5\%$. Before SEM observation, the specimens were sputter-coated with Au to avoid oxidation and any other charging effects and also to improve the electro conductivity of specimens for acquiring better SEM photos.

Ball shear test was taken to further quantify the mechanical properties of the solder joints. It was carried out by using a shear testing platform (Dage Series 4000 Bond Tester). The weight of the pendulum was 4.0 kg, the shear height was 20 μm and the shear speed was 200 μm/s. The average failure force of 30 solder balls with the minimum and maximum values removed was taken for each condition. The fracture-type and the micromorphology of the fracture surface will be confirmed after the ball shear test with the assistant of SEM observation.

3 Results and discussions

From the perspective of material types, in the solder paste, Sn57.6Bi0.4Ag near eutectic solder is a kind of solid

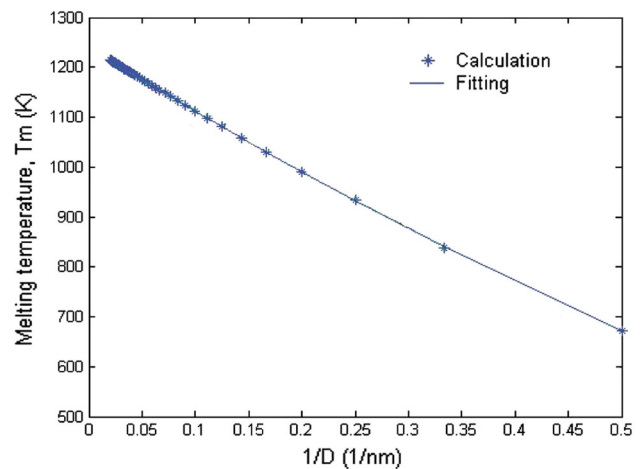


Fig. 3 Plot of relationship of melting temperature with the reciprocal of nano Ag particles diameter

solution material, but the doped Sn58Bi + 0.4Ag solder is a composite material that consists of Sn58Bi eutectic solder and nano Ag particles. For the doped Sn58Bi + 0.4Ag solder, it has characteristics of Ag nanoparticles, while Sn57.6Bi0.4Ag solder does not have these properties. Figure 3 shows the relationship between melting temperature and the reciprocal of nano Ag particles diameter [18]. The average diameter of the nano Ag particles used in this research was 70 nm. It is easily to be found that the melting temperature of nano Ag particles is much higher than 178 °C which was set as the peak temperature in the reflow process. Therefore, during the reflow process, solid–liquid reactions would happen between nano Ag particles and melted Sn58Bi solder. Nano Ag particles would gradually transform to Ag_3Sn IMCs. During this process, nano Ag and Ag_3Sn particles gathered easily, due to the high surface energy and the different density between nano Ag particles and the solder matrix. However, Ag elements have already existed in the form of Ag_3Sn IMCs in the Sn57.6Bi0.4Ag solder before reflow process, according to the phase diagram of Sn–Bi–Ag alloy in Fig. 4. The difference between these two solder materials, caused by the different way of Ag addition, must result in the different mechanical properties of the solder joints during aging.

3.1 Melting point analysis

DSC analysis was carried out in order to investigate the fundamental thermal reactions on heating of these solders. Figure 5 shows typical DSC curves obtained for Sn58Bi, Sn57.6Bi0.4Ag and Sn58Bi + 0.4Ag solders on heating. The melting temperatures were 139.9, 140.1 and 139.5 °C for Sn58Bi, Sn57.6Bi0.4Ag and the doped Sn58Bi + 0.4Ag

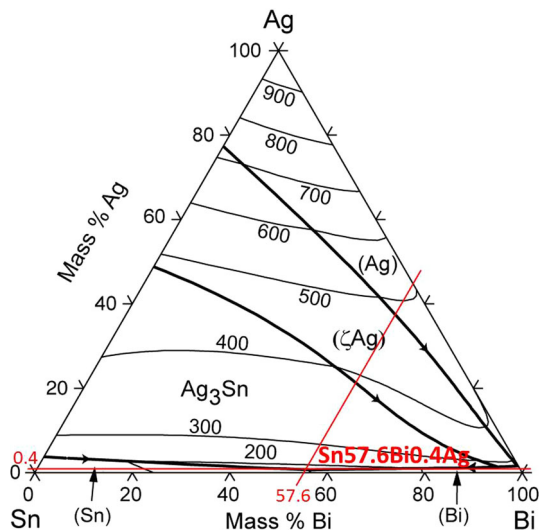


Fig. 4 The Phase diagram of Sn–Bi–Ag alloy

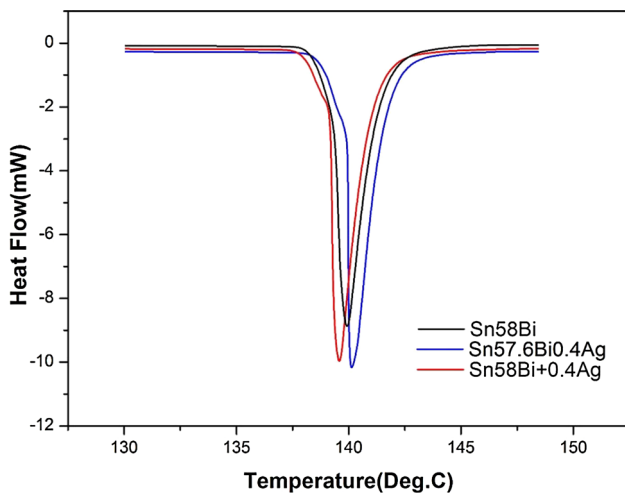


Fig. 5 DSC curves of Sn58Bi, Sn57.6Bi0.4Ag and the doped Sn58Bi + 0.4Ag solders on heating

solders, respectively. It is noteworthy that solders with Ag added need higher energy of heat flow to be melted. And there was no big difference among the melting temperatures for these solders. According to this result, it was confirmed that the same reflow program, shown in Fig. 1, can be suitable for all these tested solder pastes.

3.2 Micromorphology characterization (before aging)

Figure 6 shows backscattered scanning electron micrographs of Sn58Bi, Sn57.6Bi0.4Ag and the doped Sn58Bi + 0.4Ag solder joints, respectively. AuSn₄ IMC particles appeared in the Sn rich phase, due to the fast

diffusion of Au atoms from the outmost layer of Au/Ni/Cu pad into the solder side when experiencing the reflow process. The fast diffusion of Au ensured a good connection between the solder and Ni layer on the pad. Ni₃Sn₄ IMCs near the solder side and Ni₃Sn IMCs near the pad side were both observed at the interface of solder joints, which was confirmed by EDX analysis. And the dendritic segregation parts were detected in all solder sides, on account of the different nucleation rate between Sn and Bi phases [19]. However, according to the EDX result in Fig. 6g, it is interesting to notice that needle-shaped Ag₃Sn IMCs were only apparently observed in the doped Sn58Bi + 0.4Ag solder joints, as showed in Fig. 6e, f. Two factors might contribute to this phenomenon. For one aspect, in the doped Sn58Bi + 0.4Ag solder paste, nano Ag particles gathered easily during reflow process. Though best efforts had been done to make nano Ag particles uniformly distributed in the Sn58Bi solder when preparing the solder paste, it was beyond our control during the reflow process. For another aspect, Ag₃Sn IMCs in the Sn57.6Bi0.4Ag near eutectic solder dispersed much more uniformly. And because of the basic properties of solid solution material, these Ag atoms hardly moved away from the original positions in the grain lattices without any other strong external stress. As a result, Ag₃Sn IMCs in the Sn57.6Bi0.4Ag solder joints had not been detected to be gathered.

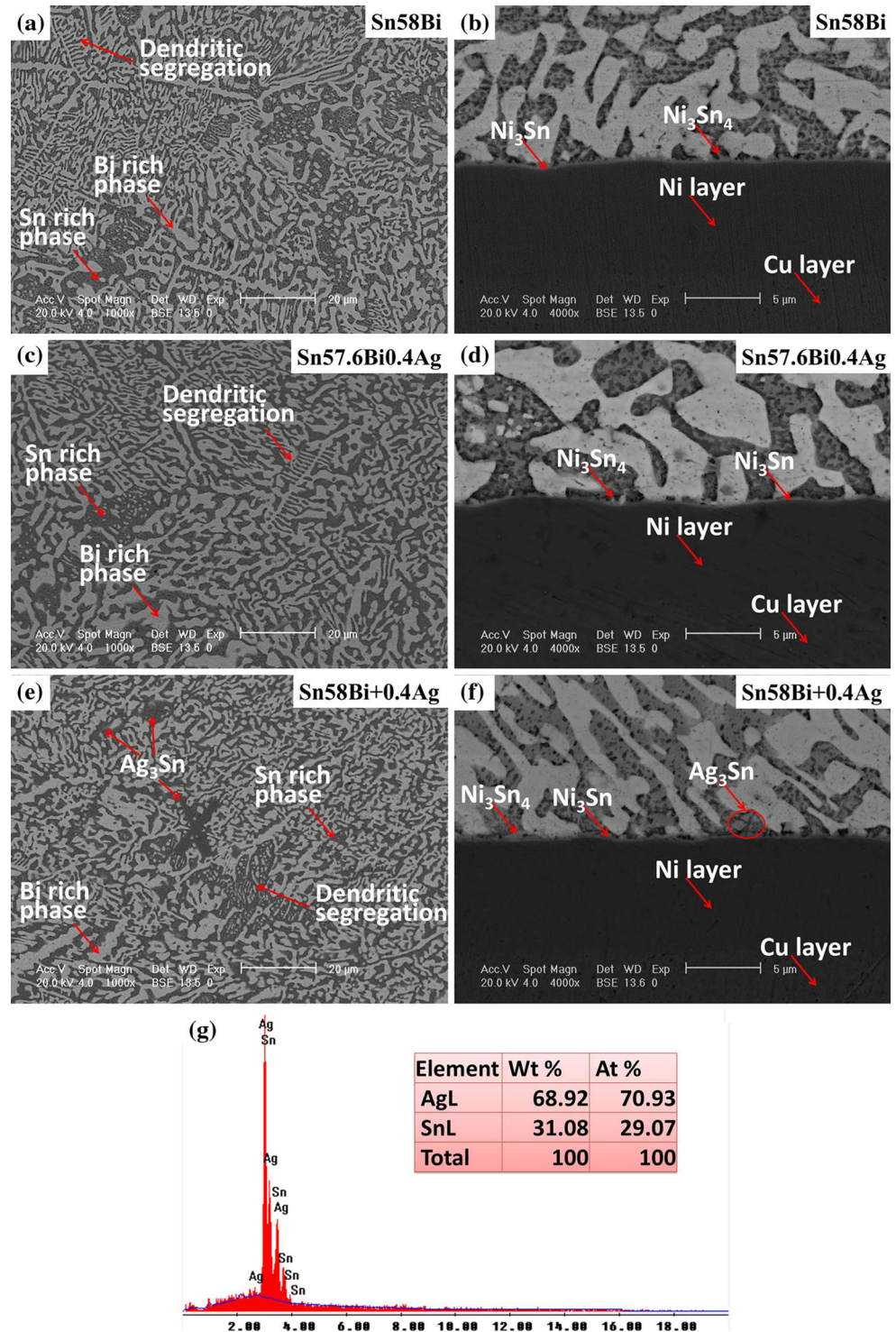
3.3 Thermal failure analysis

3.3.1 Micromorphology characterization (after aging)

Thermal aging, helping to accelerate the generation of defects and failures at the solder joints, is commonly used for testing thermal mechanical properties of solder joints. It makes experimental study more efficient. The micromorphology of Sn57.6Bi0.4Ag and the doped Sn58Bi + 0.4Ag solder joints at the solder side after 100 and 200 h aging under 100 °C are shown in Fig. 7 respectively. With the increasing of aging time, the remained nano Ag particles in the doped Sn58Bi + 0.4Ag solder joints gradually reacted with Sn phase completely and the gathering phenomenon of Ag₃Sn IMCs became more serious, as shown in Fig. 7c, d, comparing with Fig. 6e. However, until aged for 100 h, it was the first time that Ag₃Sn phases appeared in the Sn57.6Bi0.4Ag solder joints, but the grain size of these IMCs were much smaller than those in the doped Sn58Bi + 0.4Ag solder joints, as shown in Fig. 7a.

The micromorphology changes of solder/pad interfaces of Sn57.6Bi0.4Ag and the doped Sn58Bi + 0.4Ag solder joints after 100, 200 and 500 h aging were revealed in Fig. 8. As a whole, the Ni layer was gradually consumed,

Fig. 6 BSE images of cross-sectioned **a, b** Sn58Bi, **c, d** Sn57.6Bi0.4Ag, and **e, f** the doped Sn58Bi + 0.4Ag solder joints before aging; **g** EDX spectrum result of the needle-like particles in the doped Sn58Bi + 0.4Ag solder joints



and the Ni–Sn IMC layers were thickening with the increasing of the aging time. It is interesting to notice that the Ni–Sn IMC layers in the doped Sn58Bi + 0.4Ag interface were seriously unsmooth and uneven. On account of the trend of the dissolution of Ni–Sn IMCs into the solder side, huge amount of Ni–Sn IMCs moved away from

interface of the joints. The stick-like and irregular-shaped Ni_3Sn_4 IMCs were easily found on or near the bottom IMC layers in the doped Sn58Bi + 0.4Ag solder joints, as shown in Fig. 8b, d, f. A similar phenomenon was found in molten lead-free solders before, without interfacial reaction occurring between the molten Sn and the Ni_3Sn_4 phase

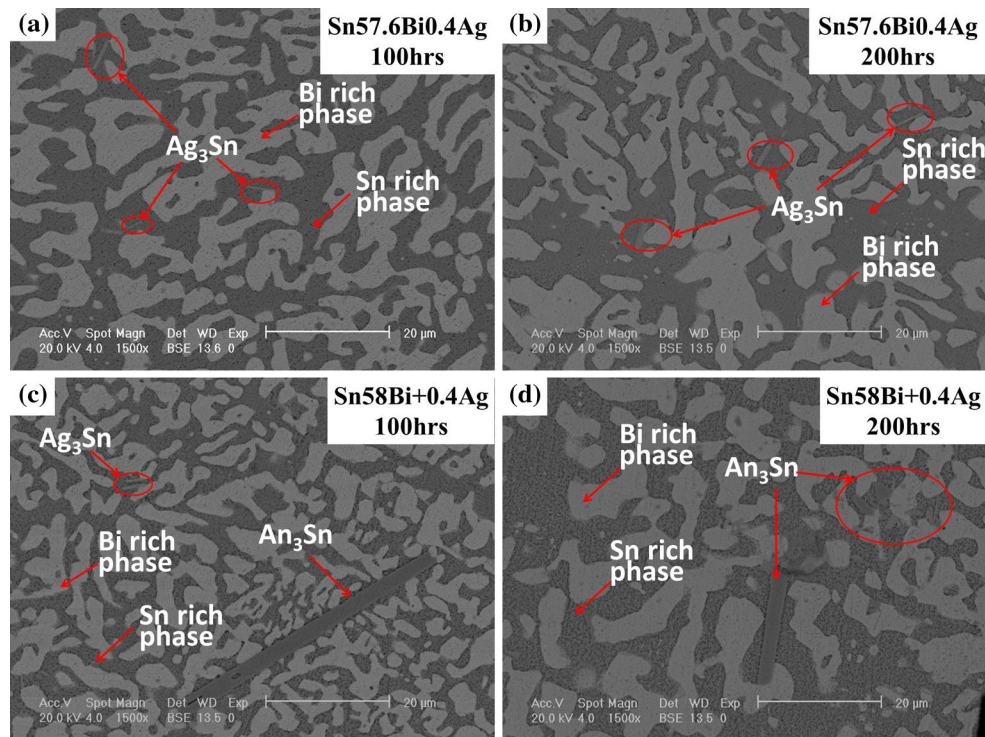


Fig. 7 BSE images of cross-sectioned **a, b** Sn57.6Bi0.4Ag and **c, d** the doped Sn58Bi + 0.4Ag solder joints after 100–200 h aging

[20]. In this research, Ni–Sn IMCs seriously dissolved into the solder side of the doped Sn58Bi + 0.4Ag solder joints under 100 °C. A possible explanation is that the excessively-gathered Ag_3Sn IMCs would create more grain boundary dislocations and defects in the solder joints, making rooms for the dissolution of Ni–Sn IMCs. It could lead to the degenerated phenomenon of Ag nanoparticle reinforcement, making the doped nano Ag particles lose their functions. In addition, Bi phase, with a higher density (9.78 g cm^{-3}) than Ni_3Sn_4 phase (8.65 g cm^{-3}), was intent to move to the bottom [21], compelling and squeezing Ni–Sn IMCs to move up, as described in Fig. 8b. Also, the 100 °C environment accelerated the moving and the diffusion phenomenon of IMCs. On the other hand, during the aging, Ni–Sn IMC layers kept staying at the bottom and becoming thicker in the Sn56.7Bi0.4Ag solder joints. No obvious phenomenon had been detected that Ni–Sn IMCs seriously dissolved into the solder side of Sn56.7Bi0.4Ag solder joints. But these Ni–Sn IMCs mixed together with the sinking Bi phase after 500 h aging, as shown in Fig. 8a, c, e. The better distribution of Ag_3Sn IMCs and the better arrangement of grain lattices helped Sn56.7Bi0.4Ag solder joints to prevent the dissolution of Ni–Sn IMCs. It implies that Sn56.7Bi0.4Ag solder joints performed better than the doped Sn58Bi + 0.4Ag solder joints in preventing the dissolution of Ni–Sn IMCs into the solder side.

3.3.2 The thickness of IMC layers

According to the condition in this research, the thicknesses of IMC layers at the solder/pad interfaces and the thicknesses of Ni layer in the UBM layers were both measured. Lots of efforts have been done to analyze the effect of thickness of IMC layers on the mechanical properties of the solder joints in the former researches [22]. However, in this research, huge differences were found between the changes of thickness of IMC layers in the Sn57.6Bi0.4Ag and the doped Sn58Bi + 0.4Ag solder joints. As a result, we would like to use the relationship between the consumption of Ni layer and the accumulation of IMC layers to study the effect of IMC layer changes on the mechanical properties of solder joints. This method was used for the first time in related researches. As mentioned in Sect. 3.3.1, Ni–Sn IMCs gradually dissolved into the solder side, so that the measured thicknesses of IMC layers could not represent the total formation of Ni–Sn IMCs during reflow and aging processes. Therefore, the consumption of Ni layer should be taken into consideration.

The statistical result of the thickness changes of the IMC layers at the solder/pad interfaces and the Ni layer in the UBM layers is shown in Fig. 9. It reveals that as the aging time increasing, IMC layers became thicker and Ni layer became thinner in both Sn57.6Bi0.4Ag and the doped

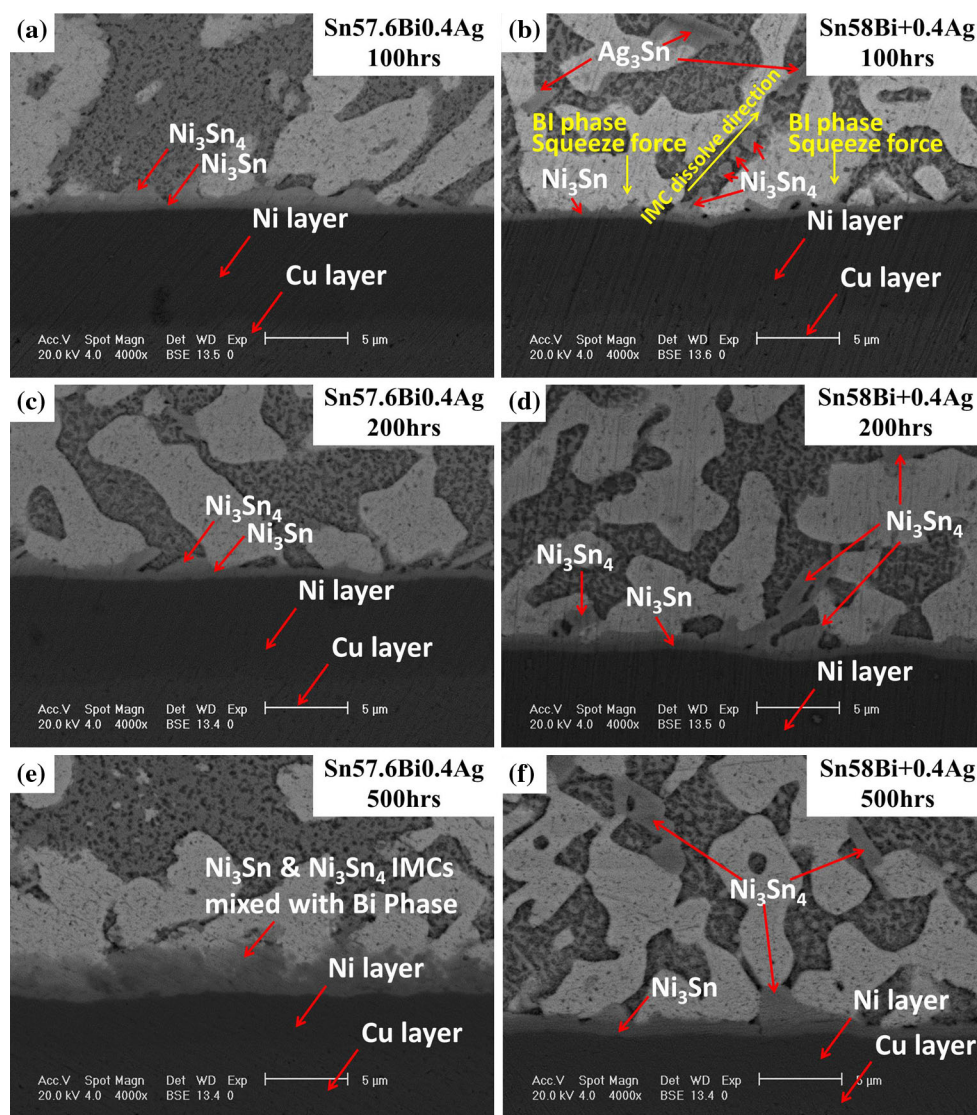


Fig. 8 BSE images of cross-sectioned **a, c, e** Sn57.6Bi0.4Ag and **b, d, f** the doped Sn58Bi + 0.4Ag solder joints after 100–500 h aging

Sn58Bi + 0.4Ag solder joints. It is interesting to notice that IMC layers accumulated much thicker in the Sn57.6Bi0.4Ag solder joints than layers in the doped Sn58Bi + 0.4Ag solder joints, but the thickness of Ni layer in the doped Sn58Bi + 0.4Ag solder joints was thinner than that in the Sn57.6Bi0.4Ag solder joints, especially after 500 h aging. Here, we defined the thickness conversion rate (TCR), which stands for the proportion of the thickness of accumulation to the thickness of consumption. TCR can be calculated by the equation:

$$\begin{aligned} \text{TCR} &= \Delta L'_t / \Delta L_t = (\Delta L'_t / t) / (\Delta L_t / t) \\ &= V_{\text{accumulation}} / V_{\text{consumption}} \end{aligned} \quad (1)$$

where t stands for the time; ΔL_t is the changes of thickness of the consumed lay; $\Delta L'_t$ is the changes of thickness of accumulated layer; $V_{\text{accumulation}}$ is the average accumulation

rate of thickness; $V_{\text{consumption}}$ is the average consumption rate of thickness.

Table 2 shows the average consumption rate of Ni layer, the accumulation rate of IMC layers, and the value of TCR for Sn57.6Bi0.4Ag and the doped Sn58Bi + 0.4Ag solder joints, during aging from 0 to 500 h.

According to the result in the Table 2, TCR of Sn57.5Bi0.4Ag solder was three times higher than the TCR of the doped Sn58Bi + 0.4Ag solder. It means that more consumed Ni layer transformed to Ni–Sn IMCs that accumulated at Sn57.5Bi0.4Ag solder joints interface than dissolved into the solder side. But for the doped Sn58Bi + 0.4Ag solder joints, more Ni–Sn IMCs would dissolve into the solder side than stay at the interface. In other word, this result proves from another angle that Sn56.7Bi0.4Ag solder joints performed better than the

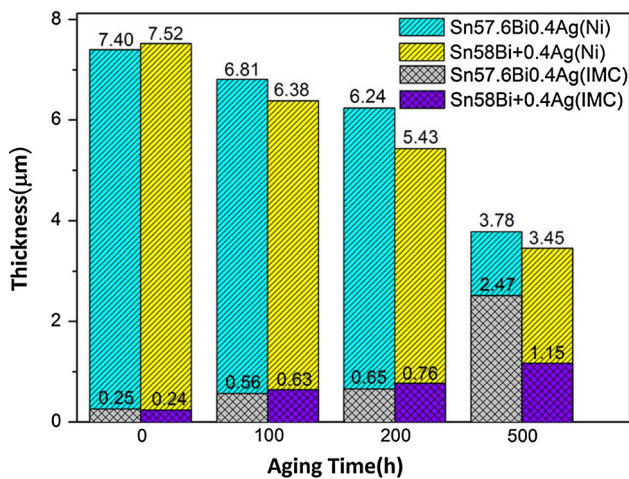


Fig. 9 The statistical result of the thickness changes of the IMC layers at the solder/pad interfaces and the Ni layer in the UBM layers

Table 2 Average velocities of consumption of Ni layer and accumulation of IMC layer between 0 and 500 h aging, respectively for Sn57.6Bi0.4Ag and the doped Sn58Bi + 0.4Ag solder joints

Solder	Ni layer consumption rate (nm/h)	IMCs layer accumulation rate (nm/h)	TCR
Sn57.6Bi0.4Ag	7.24	4.44	0.61
doped Sn58Bi + 0.4Ag	8.14	1.82	0.22

doped Sn58Bi + 0.4Ag solder in preventing the dissolution of Ni–Sn IMCs into the solder side.

Figure 10 shows the ratio of solder joints with no crack, short cracks and long cracks near the IMC layers after different aging time. According to the result, Sn57.6Bi0.4Ag solder joints showed a better performance in preventing crack formation. Not only the first crack occurring in the Sn57Bi0.4Ag solder joints formed later, but also the number of cracks was fewer, comparing with the doped Sn58Bi + 0.4Ag solder joints. And there was no long crack detected in the Sn57Bi0.4Ag solder joints, even after 500 h aging. The essence of this phenomenon was also related to the fact that IMC layers were much more stable at the interface of Sn57Bi0.4Ag solder joints, without apparent tendency of dissolution into the solder side. However, in the doped Sn58Bi + 0.4Ag solder joints, influenced by the dissolution of Ni–Sn IMCs, many long and short cracks easily generated at the interface of the solder joints.

3.4 Mechanical analysis

3.4.1 Ball shear test

Ball shear test is commonly used to evaluate the mechanical characteristics of the solder joints, and the value of ball

shear force has close relationships with the aging time, temperature and the thickness of the IMC layers. Figure 11 shows the ball shear test results for Sn58Bi, Sn57.6Bi0.4Ag and the doped Sn58Bi + 0.4Ag solder joints. Before aging, the ball shear force of the doped Sn58Bi + 0.4Ag solder joints was highest, with an average value of 10.8 N. It proves that the mechanical properties of the doped Sn58Bi + 0.4Ag solder joints were obviously improved by the dispersion of nano Ag particles. However, the ball shear force decreased fast as the increasing of the aging time. After 100 h aging, Sn58Bi, Sn57.6Bi0.4Ag and the doped Sn58Bi + 0.4Ag solder joints almost had the same ball shear forces, around 6.7 N. Thereafter, the ball shear forces of Sn58Bi and Sn57.6Bi0.4Ag solder joints gradually overpassed the doped Sn58Bi + 0.4Ag solder joints. And the force of Sn57.6Bi0.4Ag solder joints became the highest one. This degenerated phenomenon of nanoparticle reinforcement in the doped Sn58Bi + 0.4Ag solder joints was mainly caused by the sustained gathering of Ag₃Sn IMCs and the growth of the grain size during aging.

Comparing Figs. 8 and 9 with 11, it is interesting to notice that after 200 h aging, Sn57.6Bi0.4Ag solder joints with thicker IMC layer had higher ball shear force. But it does not mean this result is contrary to the well-known conclusion that the solder joints with thicker IMC layer were easier to be broken at the interface [22–24]. Because we found that the flatness at the joint interface should be the major factor that decided the fracture force of the solder joints in this research, but not the thickness of IMC layers. As shown in Fig. 8c–f, the interfaces were much smoother at the Sn57.6Bi0.4Ag solder joints than those at the doped Sn58Bi + 0.4Ag solder joints. Especially, after 500 h aging, IMC layer mixed with solder together at the interface of Sn57.6Bi0.4Ag solder joints, which could be regard as a kind of “mixed state”. However, the interface of the doped Sn58Bi + 0.4Ag solder joints became rougher and uneven, caused by the dissolution of Ni–Sn IMCs. The smoother surface with “mixed state” could distribute stress well, while the rougher surface might cause serious stress concentration at the protuberant IMCs. As a result, Sn57.6Bi0.4Ag solder joints with smoother joint interface had higher ball shear force than the doped Sn58Bi + 0.4Ag solder joints with rougher joint interface.

3.4.2 Fracture surface analysis

Figure 12 shows the morphology of fracture surfaces of Sn57.6Bi0.4Ag and the doped Sn58Bi + 0.4Ag solder joints after 0 and 500 h aging respectively. The fracture surface was composed of bright and dark regions. The bright region is considered to be the cleavage of solder, showing ductile characteristic; and the dark region stands for small IMC grains, showing brittle characteristic [21]. It

Fig. 10 The ratio of solder joints with no crack, short cracks and long cracks near the IMC layer after different aging time, for Sn57.6Bi0.4Ag and the doped Sn58Bi + Ag solder joints

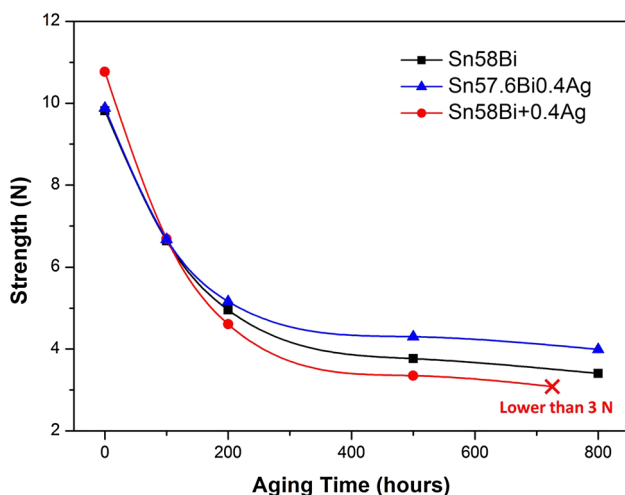
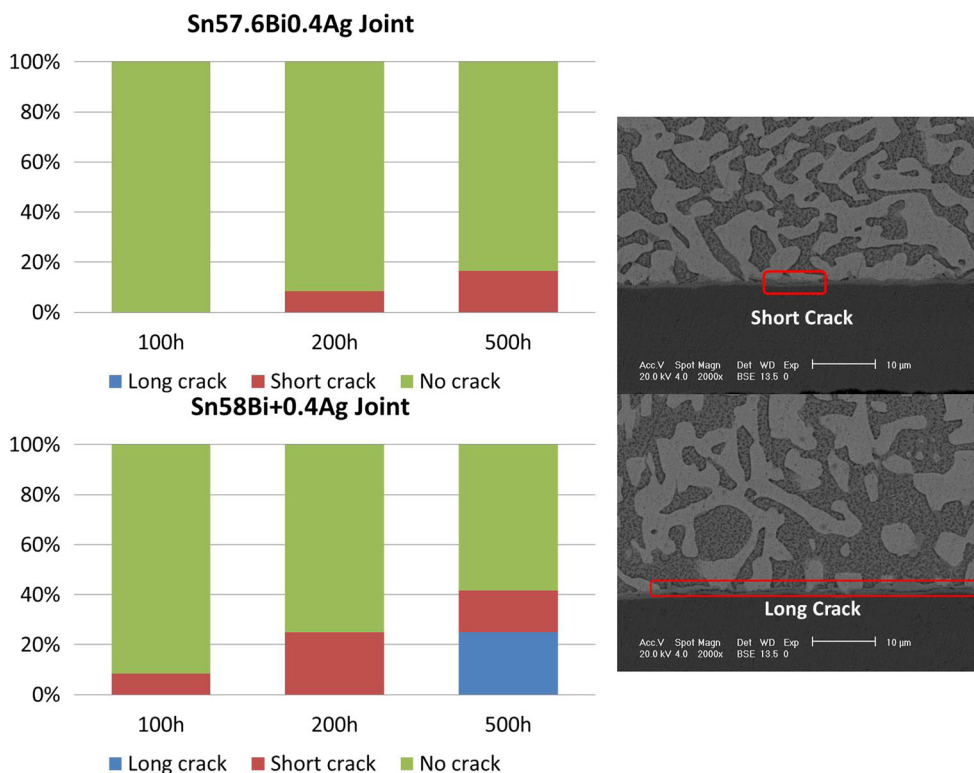


Fig. 11 Plot of the relationships of ball shear force with aging time, for Sn58Bi, Sn57.6Bi0.4Ag and the doped Sn58Bi + Ag solder joints

means that the fracture surface looks darker, the more brittle the joints should be. Before aging, most parts of fracture surface of both kinds of solder joints belonged to the bright region, as shown in Fig. 12a, b. After 500 h aging, more dark-regions were detected in the fracture surface of the doped Sn58Bi + 0.4Ag solder joints, contrasting with Sn57.6Bi0.4Ag solder joints, as shown in Fig. 12c, d. It can be concluded that the doped

Sn58Bi + 0.4Ag solder joints were more brittle than Sn57.6Bi0.4Ag solder joints after long-time aging.

4 Conclusion

Two methods of Ag addition into the Sn–Bi solder had been studied in this research. The first way (Way I) was to blend the reinforced particles with solder powders together, and then followed by pressure forming, sintering, cooling, crystallization and serious machining methods to make the Sn57.6Bi0.4Ag solder paste. And the second way was to directly distribute nano Ag particles into the Sn58Bi solder paste by sufficient mechanical-stirring, to make the doped Sn58Bi + 0.4Ag solder paste. The mechanical properties of Sn57.6Bi0.4Ag and the doped Sn58Bi + 0.4Ag solder joints during aging were shown to be associated with the changes of micromorphology, the dissolution of IMCs, as well as the flatness of the joints' interface. The addition of Ag did not influence the melting temperature of Sn58Bi solder according to the DSC curves. The reflow program used by Sn58Bi solder paste is also suitable for Sn57.6Bi0.4Ag and the doped Sn58Bi + 0.4Ag solders. Before long-time aging, the doped Sn58Bi + 0.4Ag solder joints showed better mechanical performance than Sn57.6Bi0.4Ag solder joints. During aging, Sn56.7Bi0.4Ag solder joints had better performance in preventing the dissolution of Ni–Sn IMCs into the solder side, having

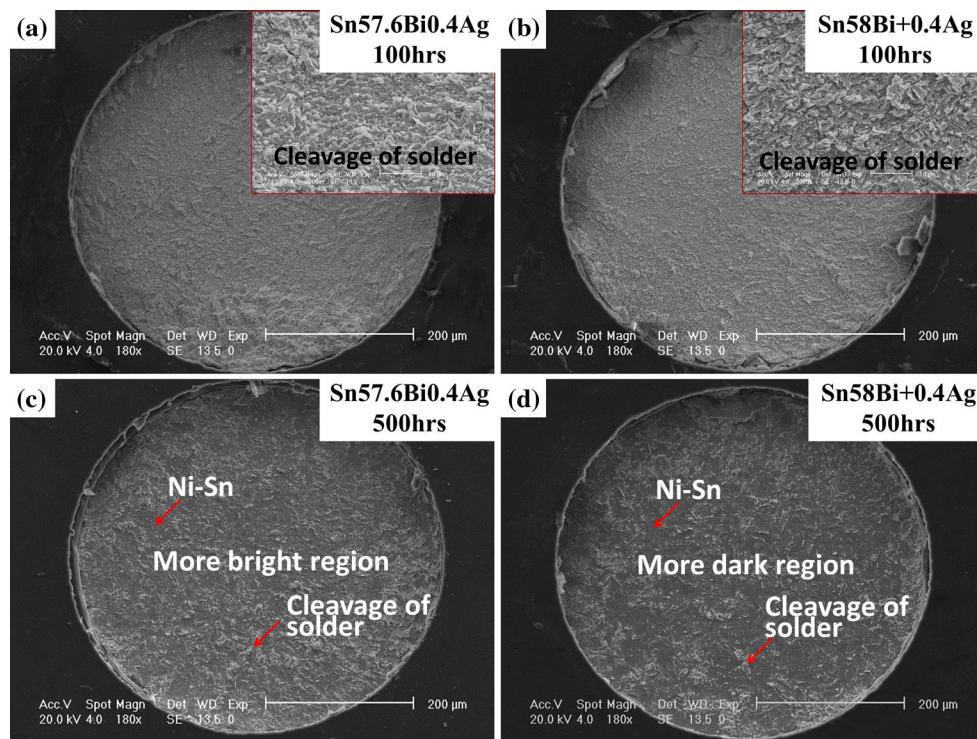


Fig. 12 SEM images of the fracture surfaces for Sn57.6Bi0.4Ag and the doped Sn58Bi + 0.4Ag solder joints after 0 and 500 h aging

smoother interfaces, comparing with Sn58Bi + 0.4Ag solder joints. The degenerated phenomenon of Ag nanoparticle reinforcement seriously happened in the doped Sn58Bi + 0.4Ag solder joints. After long-time aging, Sn57.6Bi0.4Ag solder joints had better mechanical properties than the doped Sn58Bi + 0.4Ag solder joints.

5 Future work

Based on this research of the Ag additive methods, the effectiveness of nano doping reinforcement has been questioned. It is because of the limited improvement, much higher cost, and the degenerated phenomenon when experiencing high-temperature and long-time aging. Kotadia et al. [25] also pointed out many limitations of nanoparticle enhanced solder pastes for electronics assembly. The effects of particles improvement in solder joints are decided by the content, the distribution and the size of the particles, which influenced mutually. And for Ag particles in the Sn–Bi solder, the distribution plays an important role, which is greatly influenced by additive methods.

To get a more comprehensive view of the effects of Ag additive methods into the Sn58Bi solder joints, we would like to apply high current density into the solder joints to study electrical properties.

Acknowledgments The authors would like to acknowledge the financial support provided by the National Natural Science Foundation of China/Research Grants Council of Hong Kong (NSFC/RGC), Ref. No. 9054008 (Electromigration and Thermomigration Studies in Nanostructured Composite Electronic Interconnects for Nanoelectronics Applications), and the Research Grants Council of Hong Kong, Ref. No. 9041636 (A Study of Nanostructured Electronic Interconnects-preparation, Characterization and Integration).

References

1. J.W. Yoon, B.I. Noh, S.B. Jung, Comparison of interfacial stability of pb-free solders (Sn–3.5Ag, Sn–3.5Ag–0.7Cu, and Sn–0.7Cu) on ENIG-plated Cu during aging. *IEEE. Trans. Adv. Package* **33**, 64–70 (2010)
2. Q.K. Zhang, Q.S. Zhu, H.F. Zou, Z.F. Zhang, Fatigue fracture mechanisms of Cu/lead-free solders interfaces. *Mater. Sci. Eng. A* **527**, 1367–1376 (2010)
3. J.H. Park, J.H. Lee, Y.H. Lee, Y.S. Kim, Reaction characteristics of the Au–Sn solder with under-bump metallurgy layers in optoelectronic packages. *J. Electron. Mater.* **31**, 1175–1180 (2002)
4. C.A. MacKay, W.D. von Voss, Effect of compositional changes and impurities on wetting properties of eutectic Sn–Bi alloy cased as solder. *J. Mater. Sci. Technol.* **1**, 240–248 (1985)
5. Y.C. Chan, D. Yang, Failure mechanisms of solder interconnects under current stressing in advanced electronic packages. *Prog. Mater. Sci.* **55**, 428–475 (2010)
6. Y. Jing, G. Sheng, Z. Huang, G. Zhao, Effects of 0.1 wt% Ni addition and rapid solidification process on Sn–9Zn solder. *J. Mater. Sci. Mater. Electron.* **24**, 4868–4872 (2013)

7. L. Shen, Z.Y. Tan, Z. Chen, Nanoindentation study on the creep resistance of SnBi solder alloy with reactive nano-metallic fillers. *Mater. Sci. Eng. A* **561**, 232–238 (2013)
8. J.W. Yoon, S.B. Jung, Reliability studies of Sn–9Zn/Cu solder joints with aging treatment. *J. Alloys Compd.* **407**, 141–149 (2006)
9. L. Zhang, S.B. Xue, L.L. Gao, G. Zeng, Z. Sheng, Y. Chen, S.L. Yu, Effects of rare earths on properties and microstructures of lead-free solder alloys. *J. Mater. Sci. Mater. Electron.* **20**, 685–694 (2009)
10. T. Siewert, S. Liu, D.R. Smith, J.C. Madeni, Database for solder properties with emphasis on new lead-free solders. NIST and Colorado School of Mines, Release 4.0 (2002)
11. A.A. El-Daly, A. Fawzy, S.F. Mansour, M.J. Younis, Thermal analysis and mechanical properties of Sn–1.0Ag–0.5Cu solder alloy after modification with SiC nano-sized particles. *J. Mater. Sci. Mater. Electron.* **24**, 2976–2988 (2013)
12. L.C. Tsao, Suppressing effect of 0.5 wt% nano-TiO₂ addition into Sn–3.5Ag–0.5Cu solder alloy on the intermetallic growth with Cu substrate during isothermal aging. *J. Alloys Compd.* **509**, 8441–8448 (2011)
13. X.J. Wang, Q.S. Zhu, B. Liu, N. Liu, F.J. Wang, Effect of doping Al on the liquid oxidation of Sn–Bi–Zn solder. *J. Mater. Sci. Mater. Electron.* **25**, 2297–2304 (2014)
14. Z. Yang, W. Zhou, P. Wu, Effects of Ni-coated carbon nanotubes addition on the microstructure and mechanical properties of Sn–Ag–Cu solder alloys. *Mater. Sci. Eng. A* **590**, 295–300 (2014)
15. X.D. Liu, Y.D. Han, H.Y. Jing, J. Wei, L.Y. Xu, Effect of graphene nanosheets reinforcement on the performance of SnAgCu lead-free solder. *Mater. Sci. Eng. A* **562**, 25–32 (2013)
16. T. Bakhishev, V. Subramanian, Investigation of gold nanoparticle inks for low-temperature lead-free packaging technology. *J. Electron. Mater.* **38**, 2720–2725 (2009)
17. R.M. Shalaby, Effect of silver and indium addition on mechanical properties and indentation creep behavior of rapidly solidified Bi–Sn based lead-free solder alloys. *Mater. Sci. Eng. A* **560**, 86–95 (2013)
18. K. K. Nanda1, A. Maisels, F. E. Kruis, B. Rellinghaus, Anomalous thermal behavior of gold nanostructures. *EPL* **80** (2007), 56003
19. X.W. Hu, Y.L. Li, K. Li, Z.X. Min, Effect of Bi segregation on the asymmetrical growth of Cu–Sn intermetallic compounds in CuSn–58BiCu sandwich solder joints during isothermal aging. *J. Electron. Mater.* **42**, 3567–3572 (2013)
20. Y.W. Yen, M.H. Kuo, W.K. Liou, T.N. Chu, Dissolution behaviors of the Ni and Ni₃Sn₄ phase in molten lead-free solders. *IMPACT* (2012), no. 6420288, 392–395
21. J.W. Yoon, S.W. Kim, S.B. Jung, IMC growth and shear strength of Sn–Ag–Bi–In/Au/Ni/Cu BGA joints during aging. *Mater. Trans.* **45**, 727–733 (2004)
22. P. Liu, P. Yao, J. Liu, Evolutions of the interface and shear strength between SnAgCu–xNi solder and Cu substrate during isothermal aging at 150 °C. *J. Alloys Compd.* **486**, 474–479 (2009)
23. K.N. Tu, Interdiffusion and reaction in bimetallic Cu–Sn thin films. *Acta. Metall.* **21**, 347–354 (1982)
24. J.W. Yoon, S.W. Kim, S.B. Jung, Effect of reflow time on interfacial reaction and shear strength of Sn–0.7Cu solder/Cu and electroless Ni–P BGA joints. *J. Alloys Compd.* **385**, 192–198 (2004)
25. H.R. Kotadia, A. Panneerselvam, M.A. Green, S.H. Mannan, Limitations of nanoparticle enhanced solder pastes for electronics assembly. *IEEE-NANO* (2012), no. 13045916, 1–5